A Tool-free Calibration Method for Turntable-based 3D Scanning Systems

Xufang Pang [1] **Rynson W.H. Lau** [1] **Zhan Song** [2] **Yangyan Li** [3] **Shengfeng He** [1]

[1] *Department of Computer Science, City University of Hong Kong, Hong Kong*
[2] *Shenzhen Institutes of Advanced Technology, Chinese Academy of Sciences, Shenzhen, China*
[3] *Department of Computer Science, Stanford University, U.S.A.*

Abstract

Turntable-based 3D scanners are popular, but require calibration of the turntable axis. Existing methods for turntable calibration typically make use of specially designed tools, such as a chessboard or criterion sphere, which requires extra human effort to be installed and dismounted in the calibration process. In this paper, we propose an automatic method to calibrate the turntable axis without any calibration tools. Given a scan sequence of the input object, we first recover the initial rotation axis from an automatic registration step. We then apply an iterative procedure to obtain the optimized turntable axis. This iterative procedure alternates between two steps: *refining the initial pose of the input scans* and *approximating the rotation matrix*. We have evaluated the performance of the proposed method on a structured light based scanning system.

Keywords: rotation axis, turntable calibration, tool-free, 3D scanning system, automatic registration

1. Introduction

A 3D model of a real world object can be constructed by capturing multiple partial scans of the object from different viewpoints and then aligning them into a consistent coordinate, as shown in Fig. 1. One approach to obtain multiple scans is to use a handheld scanner to scan a fixed object, which suffers from the registration problem, caused by unstable scanning motion. A more stable approach is to use a static camera to capture an object on a rotating turntable [Yang13] [Li11] [Brow08]. Using a turntable has many advantages, including easy installation, good stability and low registration cost. Once the turntable system is calibrated, the scan sequence of any object can be easily integrated into a complete model by rotating the partial scans around the calibrated turntable axis, without affected by noise, outliers, low percentage of overlap, featureless and large scales.

In spite of its advantages, turntable-based systems have one major assumption – the turntable axis is well calibrated. Numerous works have been conducted to develop techniques for turntable calibration. However, most of these techniques depend on specially designed tools, such as models with labels [Sain04], chessboard [Park05], and criterion spheres [Li11]. Extra human participation is needed to help install or dismount these attachments in the process of turntable calibration. In addition, re-calibration of the turntable axis is frequently required when, for example, the space configuration of the turntable-scanner needs to be adjusted to adapt to different sizes of objects being scanned. On the other hand, if we scan any objects without calibration, the rotation axis for the scanned data will be lost once the space configuration is changed. As such, a flexible and convenient method for turntable calibration is needed.

The main contribution of this paper is that we propose a framework to automatically calibrate the turntable axis directly from the scan sequence of the input object. An iterative procedure is applied to achieve an optimized axis. The iteration alternates between refining the input pose of fine registration

and approximating a rotation matrix to the refined registration matrix. The proposed method is able to calibrate turntable axes in a tool-free manner.

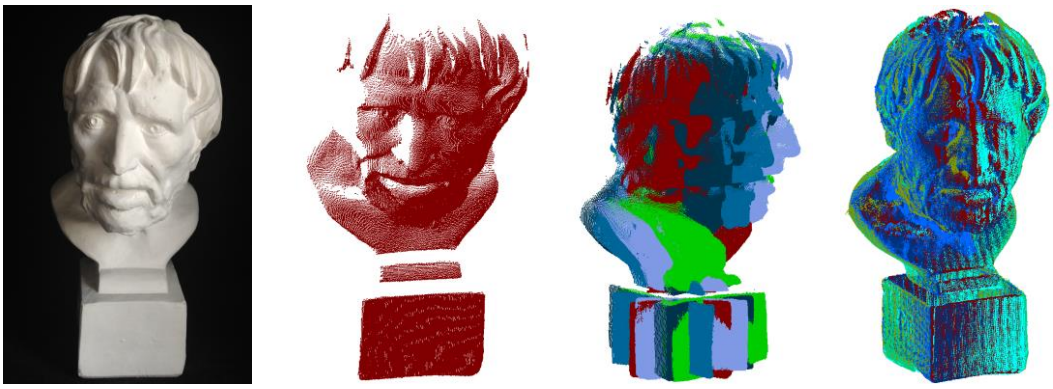

(a) (b) (c) (d)

Figure 1. Scanning results of a turntable-based scanning system: (a) photograph of the object, (b) single scan of the object, (c) multiple scans of the object, marked in different colors, and (d) output model registered based on our calibrated turntable axis.

2. Related Work

Numerous turntable calibration techniques have been proposed. For a turntable-based scanning system, the rotation axis is perpendicular to the turntable surface. Since the corresponding points (CPs) of different scans captured from different views form a plane parallel to the turntable surface, a popular turntable calibration method is to place special markers on the turntable and identify their CPs.

In [Park05], a checkerboard is used as the calibration tool to estimate the rotation axis. It computes the 3D positions of corner points of the checkerboard in different scans, and solves an over-determined linear equation to approximate the axis direction. In [Sadl05], the turntable axis is computed as the rotation axis of the fitting circle of virtual camera positions. It uses color-marked chessboard and performs extrinsic camera calibration for each scan. However, using these marked tools for calibration can be tedious. This is because, during the actual operation, the operator needs to adjust the space-configuration of the turntable and camera to make sure that the scanning range is suitable for the object, and meanwhile, for the sake of CP extraction, all valid makers on the calibration tool should be within the scanning range. In addition, the operator also needs to ensure that all markers on the tool are clearly visible as the tool is being rotated.

Other than using markers, criterion objects are also used to estimate the rotation axis based on geometry processing methods. In [Li11], a criterion sphere mounted on the turntable is used as a calibration tool. A circle is fitted to the center of the sphere captured at different angles by rotating the turntable. This step is then performed with a sphere of different size to obtain another circle. The rotation axis is defined as the line joining the centers of the two circles.

Notwithstanding the demonstrated success, a common limitation of all methods discussed above is that they all require using some specially designed tools. Extra human participation is usually required to mount or dismount the attachments. Although using markers permanently attached to the turntable [Sain04] can save the installation efforts, the scanning range may be constrained and the markers will appear in the scanning results. In [Xian04], a dynamic zoom calibration technique is proposed. It first

calibrates the rotation axes for a set of selected zoom settings. The axis parameters for other zoom settings are intersected from their nearest calibrated zoom positions. However, this method is only applicable for systems with zoom lens, and the workload on the calibration procedure is high due to its multi-calibration process. In addition, once the system is calibrated, pitching or yawing of the scanner is not allowed.

To avoid the laborious calibration task of existing scanning systems, we propose an automatic method to determine the rotation axis from only the 3D scan sequence of the input object. Our method first registers an image pair of the scan sequence to recover the initial turntable axis from the registration result. The turntable axis is then optimized by iteratively approximating a rotation matrix to the refined registration matrix. In summary, our method has two advantages. First, it does not require any tools or extra human efforts. Second, turntable calibration and object registration can be accomplished together from a single scan sequence.

3. Overview of the Proposed Turntable Calibration Framework

Although the proposed turntable calibration method can be applied to general turntable-based scanning systems, our discussion is based on the use of a structured light based scanning system. This system consists of a camera and a structured light projector, as shown in Fig. 2. In each scan, a number of grey-coded structured light patterns are projected to the object. The depth for each surface point is computed by optical triangulation of the camera ray and the corresponding projector ray [Chen08]. Fig. 1(b) shows the point cloud of a single scan. To eliminate noise and outliers on the background scene, we use a simple method by putting black clothes around the scanning object to absorb light, as shown on the right of Fig. 2. Hence, our system can work either under normal day light condition or in the dark.

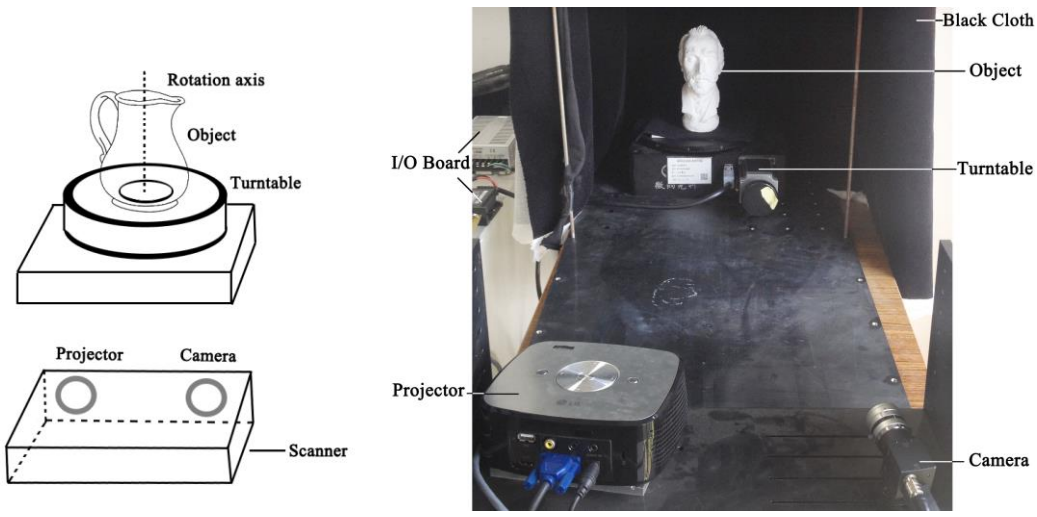

Figure 2. The structured light based scanning system.

To reconstruct a 3D model of a real object, we capture a sequence of partial scans of the object from different viewpoints, using a turntable for changing the object orientation. In all our experiments, we set the rotation angle for each scan as $\theta = 30^{o}$. Thus, a total of 12 scans are captured for each object. The scan sequence is denoted as $S = \{s_i \mid i=1,2,\ldots,12\}$, where s_i denote the point cloud of the i^{th} scan. Fig. 1(b) shows the point cloud of a single scan, and Fig. 1(c) shows all the scans (in different colors)

of the object captured from different viewpoints. Fig. 1(d) shows the scan sequence aligned in a consistent coordinate system to form a 3D model.

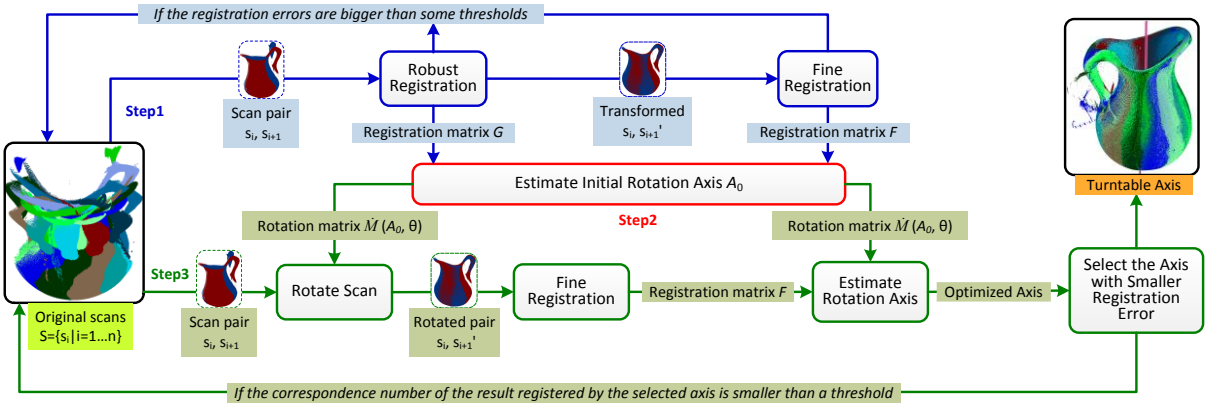

Figure 3. The proposed turntable calibration framework consisting of three steps. The first step (colored in blue) obtains one pair of well-registered scans from robust and fine registrations. The second step (colored in red) estimates the initial rotation axis from registered results. The third step (colored in green) optimizes the initial rotation axis through an iterative procedure. Note that s_i, s_{i+1} are two successive scans, s_i, s_{i+1}' denote the transformed/rotated scan pair, and $\dot{M}(A_0, \theta)$ is a rotation matrix describing a rotation around axis A_0 by θ.

The proposed method is composed of three main steps:

- First, we apply automatic robust registration and fine registration to obtain a well-registered scan pair from a sequence. See processes colored in blue in Fig. 3.
- Once obtained the registered scan pair, we approximate a rotation matrix to the registration matrix, and then compute the initial rotation axis of the turntable. See the process colored in red in Fig. 3.
- Finally, we optimize the initial axis through an iterative procedure, which alternates between refining the input pose of fine registration and approximating a rotation matrix to the refined registration matrix. See processes colored in green in Fig. 3.

We describe these three main steps in detail in the following three sections.

4. Automatic Registration of Two Successive Scans

As the scan sequence captured by the turntable-based-system is constrained to an axis rotation with a fixed rotation angle θ, one key feature is that all the successive scan pairs of the sequence can be registered by rotating them around the turntable axis by θ. Theoretically, a single well-registered scan pair is enough to recover the rotation matrix.

Robust Registration: We first apply 4PCS [Aige08] to automatically register the scan pair. In 4PCS, the best aligning rigid transform, which brings the scan pair close in a least square sense, is computed from the extracted corresponding coplanar-bases (4-coplanar-point sets) in the two scans. This method is known to be resilient to noise and outliers.

A key point of 4PCS is to use a wide-base invariant to efficiently and reliably determine rigid transformation in 3D. It is proved that alignment with wide-base is more stable than alignment using narrow-base [Aige08]. However, the width of the bases is restricted by the extent of overlap between

the scans. Hence, an overlapping fraction f for estimating the maximum distance is applied in 4PCS. Since our scans are constrained to the axis with a fixed rotation angle θ and each scan covers approximately half of the object surface, we can estimate the maximum overlapping fraction as: $f = (180 - \theta) / 180$. Thus, given two successive scans s_i, s_{i+1} of an object, the transformed scan of s_{i+1}, s_{i+1}', can be robustly aligned to the fixed scan s_i by applying 4PCS.

Alignment Evaluation: We evaluate the error of robust registration by computing the number of CPs and their average distance in the registered scans, s_i and s_{i+1}'. All point pairs in s_i and s_{i+1}' with distances smaller than a threshold ω_R are defined as CPs. If the number of CPs in s_i and s_{i+1}' is larger than a threshold m_R, and their average distance is smaller than a threshold ϖ_R, then s_i, s_{i+1}' are close enough for fine registration and the corresponding 4PCS registration matrix is recorded as G_0. Otherwise, we apply robust registration to the next pair of scans, i.e., s_{i+1} and s_{i+2}, until we obtain a well-registered scan pair. In our experiments, the thresholds are set to: $\omega_R=20*\kappa$, m_R=0.5*(N*(180-θ)/180) and ϖ_R =10*κ, where κ is the average distance of the points in the point cloud and N is the number of points in the point cloud of s_i or s_{i+1}', whichever is smaller.

Fine Registration: Once the scan pair, s_i and s_{i+1}', are close enough, we apply ICP [Rusi01] to refine the output of robust registration. ICP iteratively optimizes the alignment transformation by selecting triplet pair from the two scans and picking the best alignment. Similar to 4PCS, ICP can also be interpreted meaningfully in a framework of establish-correspondence-then-register, and the wide-base advantage [Aige08] is also applicable to ICP. Thus, by using ICP, s_{i+1}' can be further aligned to s_i, and the transformed s_{i+1}' is denoted as s_{i+1}''. To evaluate the error of fine registration, the thresholds are set to: $\omega_F=10*\kappa$, m_F=0.5*(N*(180-θ)/180) and ϖ_F =5*κ. Then, if the number of CPs in s_i and s_{i+1}'' is larger than m_F and their average distance is smaller than ϖ_F, we record the fine registration matrix as F_0, and move on to the next step. Otherwise, we start over the robust registration step with the next scan pair. Here, we take advantage of the geometric variation of object surfaces that even if most scan pairs cannot be reliably registered due to the unpredictable convergence of the registration method, we can still recover the initial rotation axis from the information distributed among the scan sequence. This is because our computation of the initial axis only requires one best aligned scan pairs from the scans.

Note that we use κ as a reference length for ω_R and ω_F because our error metric for registration results is based on computing the distance of CPs, which is around κ for perfectly registered scans. Thus, using κ as a measurement unit can intuitively indicate the closeness of the aligned scans. We use the number of overlapping points between two scans as a reference number for m_R and m_F because for perfectly registered scans the number of CPs should approximately equal to the number of overlapping points. Hence, using the number of overlapping points as a reference number here can intuitively evaluate the quality of the detected CPs as a whole. The constant coefficients of these four threshold parameters were determined empirically.

5. Estimation of the Initial Rotation Axis

The rotation axis A of the turntable can be defined by a point $P(a, b, c)$ and a vector $V(u, v, w)$. Let M be a rotation matrix that describes a rotation of angle θ around turntable axis $A(P, V)$. The initial rotation axis $A_0(P, V)$ of the turntable can be estimated by approximating M to the matrix multiplication of G_0 and F_0. According to the Rodrigue's rotation formula [Koks06], the matrix for a rotation of angle θ about an axis of direction $V(u, v, w)$ is determined as:

$$R(V,\theta) = I\cos\theta + \sin\theta[V]_{\times} + (1-\cos\theta)V \otimes V \quad (1)$$

where $[V]_x$ is the cross product matrix of V, $\otimes$ is the tensor product and I is the identity matrix. $[V]_x$ and $V \otimes V$ are defined as:

$$[V]_{\times} = \begin{bmatrix} 0 & -w & v \\ w & 0 & -u \\ -v & u & 0 \end{bmatrix} \quad \text{and} \quad V \otimes V = \begin{bmatrix} u^2 & uv & uw \\ uv & v^2 & vw \\ uw & vw & w^2 \end{bmatrix}$$

Thus, M can be computed as:

$$M(A,\theta) = \begin{bmatrix} m_{11} & m_{12} & m_{13} & m_{14} \\ m_{21} & m_{22} & m_{23} & m_{24} \\ m_{31} & m_{32} & m_{33} & m_{34} \\ m_{41} & m_{42} & m_{43} & m_{44} \end{bmatrix} = \begin{bmatrix} u^2 + (v^2+w^2)\cos\theta & uv(1-\cos\theta) - w\sin\theta \\ uv(1-\cos\theta) + w\sin\theta & u^2 + (v^2+w^2)\cos\theta \\ uw(1-\cos\theta) - v\sin\theta & vw(1-\cos\theta) - u\sin\theta \\ 0 & 0 \end{bmatrix} \quad (2)$$

$$\begin{bmatrix} uw(1-\cos\theta) + v\sin\theta & (a(v^2+w^2) - u(bv+cw))(1-\cos\theta) + (bw-cv)\sin\theta \\ vw(1-\cos\theta) - u\sin\theta & (b(u^2+w^2) - v(au+cw))(1-\cos\theta) + (cw-av)\sin\theta \\ u^2 + (v^2+w^2)\cos\theta & (c(u^2+v^2) - w(aw+bv))(1-\cos\theta) + (aw-bv)\sin\theta \\ 0 & 1 \end{bmatrix}$$

In a turntable-based scanning system, the difference between scans s_i and s_{i+1} is a rotation of around turntable axis $A(P, V)$ by angle θ. Thus, scans s_i and s_{i+1} can be registered by multiplying $M(A, \theta)$ to scan s_{i+1}. As we have used robust and fine registrations to register scans s_i and s_{i+1} with s_i fixed, the matrix multiplication of G_0 (robust registration matrix) and F_0 (fine registration matrix), where the product is denoted as W, should be equal to $M(A, \theta)$ in the perfect situation. Therefore:

$$M(A,\theta) = G_0 F_0 = W = \begin{bmatrix} w_{11} & w_{12} & w_{13} & w_{14} \\ w_{21} & w_{22} & w_{23} & w_{24} \\ w_{31} & w_{32} & w_{33} & w_{34} \\ w_{41} & w_{42} & w_{43} & w_{44} \end{bmatrix} \quad (3)$$

It is proved that any transformation can be decomposed into a translation and a rotation. However, in our case, the rotation angle is fixed and known, and robust and fine registrations involve a set of Euclidean actions of rotation and transformation in the camera coordinate. Thus, there is a high chance that the complete set of motion W cannot be decomposed into a translation and a rotation with fixed angle about a rotating axis. Hence, an optimization method for approximating $M(A, \theta)$ to W is needed.

First, the axis direction V is computed from the sub-matrices of W and M, which describe the rotation and are denoted as R_W and R_M. As mentioned in [Arfk85], for any rotation matrix R, a vector V parallel to its rotation axis must satisfy $RV=V$, which can be rewritten as $(R-I)V=0$. Then, V is computed as one of the eigenvectors of R, which corresponds to the eigenvalue $\lambda=1$ [Arfk85]. In our method, we compute $V(u, v, w)$ by simply solving the following equations due to the specific properties of the rotation matrix:

$$\begin{cases} m_{21} - m_{12} = w_{21} - w_{12} \\ m_{13} - m_{31} = w_{13} - w_{31} \\ m_{32} - m_{23} = w_{32} - w_{23} \end{cases} \quad (4)$$

With a known rotation direction, the next step is to determine point $P(a, b, c)$. The transformation is computed by solving the following three equations.

$$\begin{cases} m_{14} = w_{14} \\ m_{24} = w_{24} \\ m_{34} = w_{34} \end{cases} \tag{5}$$

Since θ and V are known, we rearrange Eq. (5) into a linear equation system of $M_T P = W_T$ as follows:

$$\begin{bmatrix} (1-\cos\theta)(v^2+w^2) & w\sin\theta-(1-\cos\theta)uv & -v\sin\theta-(1-\cos\theta)uw \\ -w\sin\theta-(1-\cos\theta)uv & (1-\cos\theta)(u^2+w^2) & u\sin\theta-(1-\cos\theta)vw \\ v\sin\theta-(1-\cos\theta)uw & -u\sin\theta-(1-\cos\theta)vw & (1-\cos\theta)(u^2+v^2) \end{bmatrix} \begin{bmatrix} a \\ b \\ c \end{bmatrix} = \begin{bmatrix} w_{14} \\ w_{24} \\ w_{34} \end{bmatrix} \tag{6}$$

If the rank of M_T is equal to 3, then point P can be uniquely determined and Eq. (6) can be solved by using LU decomposition. However, as mentioned above, W represents multiple rotation and transformation operations. Thus, with a known rotation axis and a fixed rotation angle, there is a high chance that Eq. (3) is inconsistent.

In our method, Eq. (6) is solved by computing the intersection of three planes, which are defined by the three equations. The three possible solutions are described as follows:

1. If three planes intersect at one point as shown in Fig. 4(a), the intersection point P is the unique solution.
2. If three or two planes are parallel to each other as shown in Fig. 4(b), no solutions exist.
3. If three planes intersect by one or three lines, i.e., the normal of the three planes are parallel to a reference plane, there is a unique solution for P as shown in Fig. 4(c). For the former situation, P is computed as the intersection point of the intersecting line and the reference plane. For the latter situation, a triangle is defined by the intersection points of the three intersecting lines and the reference plane. Thus, P is computed as the incenter of the triangle.

In our experiments, all P's are computed from solution 3 above. Finally, with known rotation center P and rotation direction V, the initial axis A_0 can be determined.

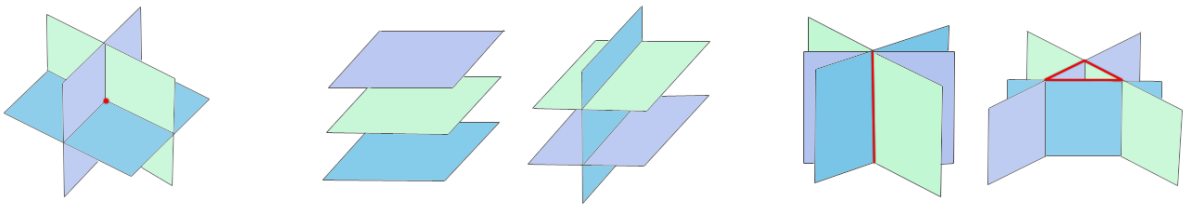

(a) (b) (c)

Figure 4. Computing point P. (a) If three planes intersect at one point, P can be uniquely determined. (b) If three or two of the planes are parallel to each other, there are no solutions for P. (c) If three planes intersect at a common line (red), P is defined as any point on the intersecting line. If three planes intersect at three different lines, P is computed as the incenter of the triangle (red).

6. Optimization of the Rotation Axis

Once we have obtained the initial turntable axis $A_0(P, V)$, the matrix for a rotation about A_0 by angle θ

can be computed according to Eq. (2), denoted as $\dot{M}_0$. Then, the next two scans s_{i+1}, s_{i+2} can be roughly aligned by multiplying $\dot{M}_0$ to scan s_{i+2}. For each point $p(x, y, z)$ in s_{i+2}, its transformed point p' can be computed as:

$$p' = \dot{M}_0 p = \begin{bmatrix} (a+(v^2+w^2)-u(bv+cw-ux-vy-wz))(1-\cos\theta)+x\cos\theta+(-cv+bw-wy+vz)\sin\theta \\ (b+(u^2+w^2)-v(au+cw-ux-vy-wz))(1-\cos\theta)+y\cos\theta+(cu-aw+wx-uz)\sin\theta \\ (c+(u^2+v^2)-w(au+bv-ux-vy-wz))(1-\cos\theta)+z\cos\theta+(-bu+av-vx+uy)\sin\theta \end{bmatrix} \quad (7)$$

Then, the roughly aligned scans s_{i+1}, s_{i+2}' are refined using the ICP method, and thus a new fine registration matrix F_1 is obtained. By approximating a new rotation matrix M to the multiplication matrix of $\dot{M}_0$ and F_1, a new optimized axis $A_1(P, V)$ is obtained.

Since the fine registration is sensitive to the initial position and may converge to a local optimal, error evaluations for axis $A_0(P, V)$ and $A_1(P, V)$ are performed to find a better axis. Similar to the computation of $\dot{M}_0$, the rotation matrix of $A_1(P, V)$ is computed and denoted as $\dot{M}_1$. According to the Eq. (7), we separately register successive scans s_{i+2} and s_{i+3} by using $\dot{M}_0$ and $\dot{M}_1$. Then, their registration errors are measured by finding the CPs of the registered scans s_{i+2} and s_{i+3}'. If the distance between a point pair is smaller than threshold $10*\kappa$, the point pair is defined as a CP. One feature of the global optimal for ICP is the number of CPs in the registered scans. Thus, the axis with more CPs is selected as a better axis for the next optimization step.

To overcome the limitation of fine registration, which relies on the initial pose of the input scans, each time, the selected axis is used for robust registration of the next pair of successive scans, and thus, the initial pose of the input scans to ICP is iteratively refined by rotating the scans around the optimized axis. For example, if $A_1(P, V)$ is the better axis, then $\dot{M}_1$ is used in robust registration of s_{i+2} and s_{i+3} for the next optimization step.

Thus, the final rotation axis is obtained by iteratively refining the initial turntable axis. Then, the complete 3D model of the target object can be obtained through successively rotating the original scan sequence around the computed rotation axis by angle θ.

7. Results and Evaluations

We have implemented the proposed calibration method on a structured-light-based turntable system, and evaluated the accuracy of the computed turntable axes by estimating the registration errors of the scanned models.

Qualitative Evaluation: We first visually evaluate the proposed calibration method. In Fig. 5, we capture 12 scans of the input jar as shown in Fig. 5(b) and align them using the proposed calibration method as shown in Fig. 5(c). Fig. 5(f) compares a magnified region of the photograph of the jar (left) with that of the reconstructed model (right). We can see that all the scratches on Jar are recovered, due to the accurate registration. Fig. 5(g-l) show the reconstruction of the Van Gogh aligned with the calibrated turntable axis. Fig. 5(m-q) show the reconstruction of Flower Pot. We can see that both the geometric and texture information are reconstructed well. All these experiments show that the registration errors of the models are low enough to preserve the detail features.

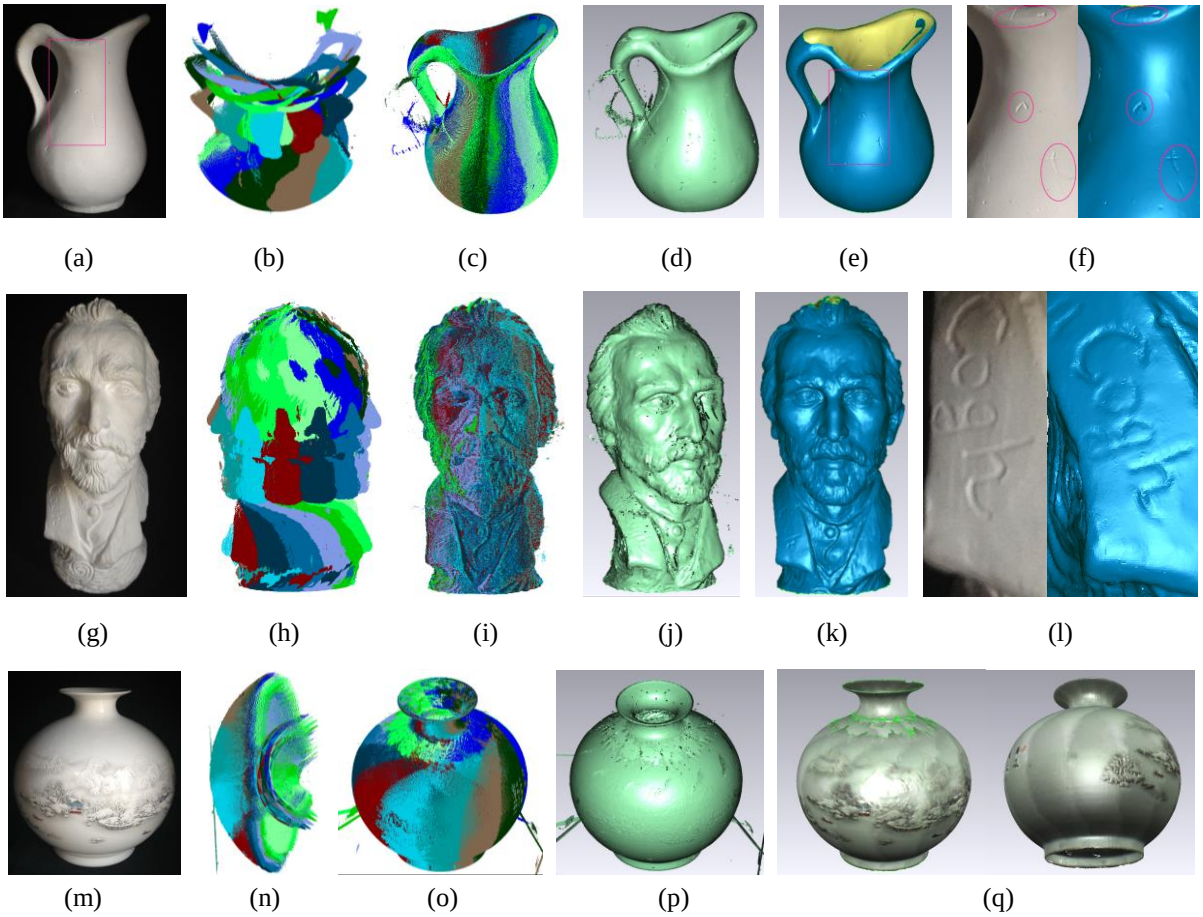

Figure 5. The Jar model registered by our calibration method. (a) input Jar, (b) scan sequence of Jar, (c) registered result, (d) rendering of the point cloud, (e) rendering of the triangulated model, and (f) the small scratches on input Jar (left) are well preserved in our reconstructed surface (right). (g) input Van Gogh statue, (h) scan sequence of Van Gogh, (i) registered result, (j) rendering of the point cloud, (k) rendering of the triangulated model, (l) comparison of local details on the real object (left) and reconstructed surface (right). (m) input Flower Pot, (n) scan sequence of Flower Pot, (o) registered result, (p) rendering of the point cloud. (q) rendering of the triangulated model with texture. We can see that the texture on the aligned model is very clear due to the accurate registration.

Quantitative Evaluation: We have also quantitatively examined the computed turntable axes using different input objects and different space configurations of the turntable scanner, as shown in Table 1. These axis coordinates are relative to the camera coordinate. Note that the computed axes are not exactly parallel to the *y* axis of the camera coordinate due to the shooting angles. Fig. 6 visually depicts the registration errors, which are defined by the distances between CPs on the registered scans. Table 2 summarizes the errors in detail, in terms of maximum error, average error, and standard deviation of CPs. Fig. 6(b) shows Jar, David and Van Gogh scanned in the same space configuration and registered using axis *A1* in Table 1, which is calibrated from Jar. Table 2 shows that the registration errors of these three plaster objects are small. Fig. 6(c) shows Van Gogh and Flower Pot scanned in the same space configuration and registered using axis *A2*, which is calibrated from Van Gogh. We can see that in Table 2, the registration error for Flower Pot is slightly higher as it is made of enamel, which has the refraction problem. Fig. 6(d) shows Horse registered using axis *A3*, which is also calibrated from Horse. We can see from Table 2 that the average distance κ of Horse is much

higher than other objects. This is because Horse is made of metal that causes strong reflection, upsetting the locations of the points in the point cloud. In general, Table 2 shows that objects captured in a space configuration with larger distance between the turntable axes and the scanner (referring to the z values in $P(x, y, z)$ of Table 1), cause higher registration errors. This is due to the fact that as the distance between the turntable axis and the scanner increases, the resolution of the point cloud becomes lower and hence, the distances between CPs generally increase. We can also see that the CP ratio, which is defined as the ratio of the number of CPs to the number of points in s_1, for models in Table 2 is around 80%, which is similar to the overlapping fraction f. This means that almost all the points that appear in both scans can be extracted as CPs. In addition, from Table 2, we also see that the average error for all models is smaller than 2κ. This shows that our turntable calibration method is robust to noise and the computed turntable axes have high accuracy.

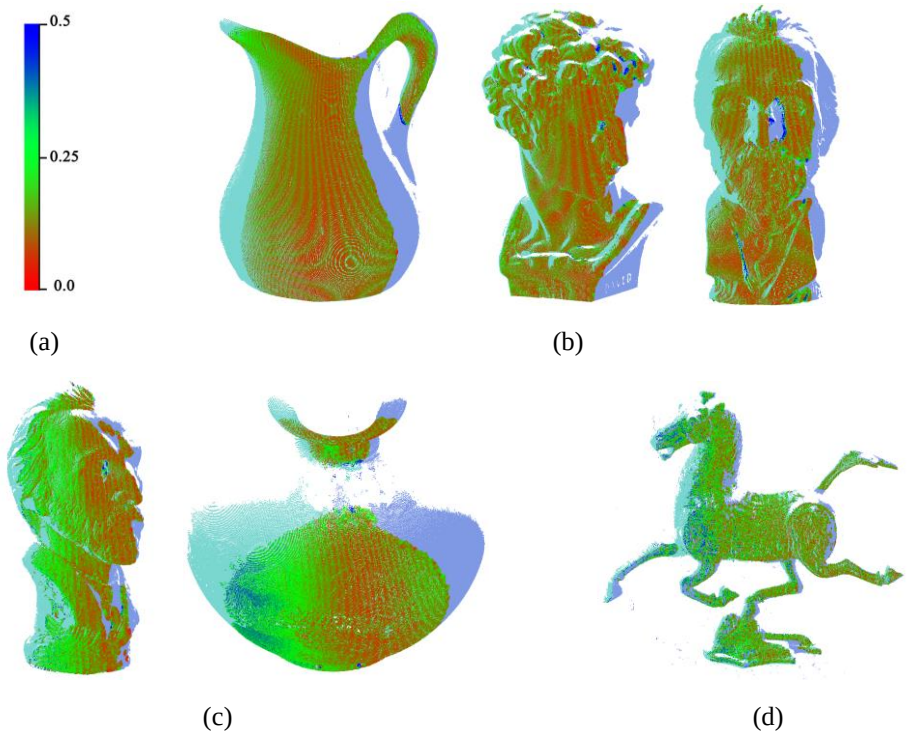

Figure 6. The registration error of two successive scans are defined by the distances of their CPs and visually depicted by colors. (a) The color bar represents the visual measure of the registration error. (b-c) show three groups of objects, registered using axes *A1*, *A2* and *A3*, respectively.

Table 1. Three turntable axes computed from the scans of the calibration objects in different space configurations of the scanner system. The computed turntable axes are defined by point P and direction vector V.

Axis	**Calibration Object**	***P*(x, y, z)**			***V*(x, y, z)**		
		x	y	z	x	y	z
A1	Jar	-14.926	80.278	581.509	0.011	0.990	-0.136
A2	Van Gogh	-14.262	120.799	751.426	0.010	0.987	-0.158
A3	Horse	0.241	123.278	782.509	0.011	0.987	-0.155

Table 2. The registration errors, including maximum error, average error and standard deviation, of the scans aligned by our calibrated axes *A*1, *A2* and *A3*.

Axis	***A1***			***A2***		***A3***
Model	Jar	David	Van Gogh	Van Gogh	Flower Pot	Horse
Number of points in s_1	321K	141K	148K	100K	431K	172K
Number of points in s_2	301K	154K	145K	108K	423K	164K
Number of CPs	234K	117K	115K	83K	356K	152K
Average distance κ	0.148	0.157	0.123	0.276	0.283	2.933
Maximum error	1.095	1.178	1.276	1.634	1.683	1.209
Average error	0.114	0.123	0.124	0.207	0.314	0.264
Standard deviation	0.044	0.062	0.075	0.101	0.407	0.154

Table 3. Comparison between the sphere-based method [Li11] and our calibration method. $A(P, V)$ denotes the rotation axis of the turntable. The object used is Jar. The average distance κ of Jar is 0.348. The numbers of points in the two scans are 101K and 106K.

Method	Rotation Axis $A(P,V)$						Number of CPs	Maximum Error	Average Error	Standard Deviation
	Point P(x, y, z)			Direction V(x, y, z)						
[Li11]	-6.739	-2.387	786.567	0.004	0.984	-0.176	86K	1.855	0.597	0.270
Ours	-4.924	143.076	759.527	0.002	0.983	-0.183	88K	1.766	0.197	0.116

Comparison: Finally, we compare our turntable calibration method with the sphere-based calibration method [Li11], which uses a criterion sphere mounted on the turntable as a calibration tool. By obtaining two scan sequences of the criterion sphere at different heights (Fig. 7(a)), two circles can be fitted to the sphere centers. The rotation axis is then defined as the line passing through the centers of the two circles, as shown in Fig. 7(b).

Table 3 shows results of the comparison. We use Jar for both calibration and testing. We can see that the registration error of our method is smaller than that of the sphere-based method. In addition, our method can also obtain a higher number of CPs. Note that during the experiment, our method does not need to mount or dismount the calibration tool. We simply scan the target object, and use the same scan sequence to compute the turntable axis as well as for model reconstruction.

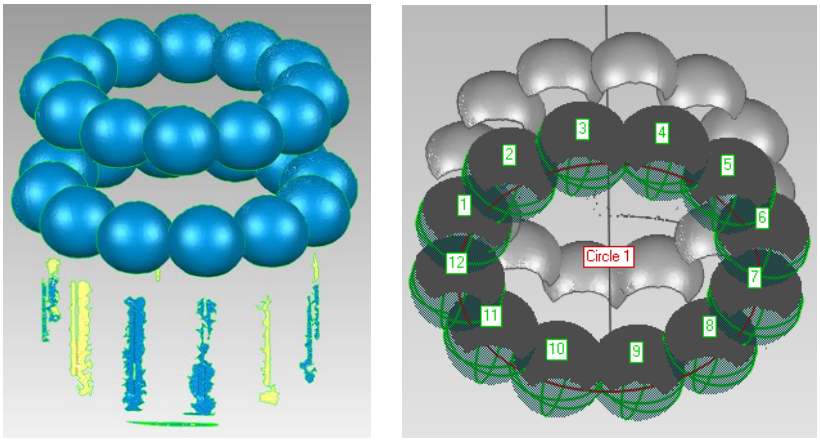

(a) (b)

Figure 7. The sphere-based turntable calibration method [Li11]. (a) Two scan sequences of criterion spheres in different heights. (b) Sphere centers are computed and fitted with two circles at different heights. The rotation axis is defined as the line joining the centers of the two circles.

Discussion and Limitations: There is one note regarding the setting of sampling angle θ. In general, using a large θ would produce scans with low overlapping fraction, resulting in the loss of the wide-base advantage [Aige08] due to the reduction of CPs, and poor initial poses for registration, resulting in a less stable registration process and a slow converging process. On the other hand, using a small θ would certainly improve the converging speed and the accuracy of registration process, as it provides better initial poses and more CPs. However, it will also produce large models, due to a large number of data points. Thus, we use $\theta = 30^o$ in our experiments, as the scanned data are sufficient to fully cover the object surface while, at the same time, the scale of the point cloud and the registration accuracy are both acceptable according to our empirical study.

The proposed turntable calibration method applies robust and fine registrations to recover the rotation matrix from two successive scans. However, existing robust and fine registration methods are not good at aligning scan sequences of slippable, flat and featureless objects, as the resulting alignment may be sub-optimal in the direction of slippage or converge to a local optimum. As a result, such kind of objects is not suitable for use as calibration objects. In addition, as the scanning system may not be able to handle objects made of highly reflective/transparent materials, these objects may also not be suitable for use as calibration objects.

8. Conclusion

In this paper, we have introduced our tool-free turntable calibration method. It is based on an iterative procedure of two steps, refining the initial pose and approximating the rotation matrix. While the proposed method does not require any tools or extra human efforts, there is also no need to perform a separate calibration process. The sequence obtained from the scanning object can be used both for calibration as well as for registration. In addition, as the proposed method only requires a scan sequence of the scanning object for calibration, it can be applied to any kind of turntable-based scanners, such as stereo-based, structured-light-based and laser. As a future work, we are considering to develop a registration technique specifically designed for scan data obtained from turntable-based scanners, to take advantage of the fact that the input scans are constrained to an axis rotation.

Acknowledgement

We would like to thank the reviewers for their insightful comments and suggestions. The work described in this paper was partially supported by a GRF grant from the RGC of Hong Kong (RGC Reference No.: CityU 115112), a SRG grant from City University of Hong Kong (Project No.: 7002768), the National Natural Science Foundation of China (No. 61375041), Shenzhen Science Plan (No. JCYJ20120903092425971 and JCYJ20130402113127502) and the Shenzhen Key Lab for Computer Vision and Pattern Recognition (No. CXB201104220032A).

References

[Aige08] D. Aiger, N. Mitra, and D. Cohen-Or. 4-points congruent sets for robust surface registration. *ACM Trans. on Graphics*, **27**(3), 2008.

[Arfk85] G. Arfken, H. Weber, and F. Harris. *Mathematical methods for physicists*, Academic Press, 1985.

[Brow08] B. Brown, C. Toler-Franklin, D. Nehab, M. Burns, D. Dobkin, A. Vlachopoulos, C. Doumas, S. Rusinkiewicz, and T. Weyrich. A system for high-volume acquisition and matching of fresco fragments: Reassembling Theran wall paintings. *ACM Trans. on Graphics*, **27**(3), 2008.

[Chen08] X. Chen, J. Xi, T. Jiang, and Y. Jin. Research and development of an accurate 3D shape measurement system based on fringe projection: Model analysis and performance evaluation. *Precision Engineering*, **32**(3):215 – 221, 2008.

[Koks06] D. Koks. A roundabout route to geometric algebra. *Explorations in Mathematical Physics*, Springer, pp. 147–184, 2006.

[Li11] J. Li, M. Chen, X. Jin, Y. Chen, Z. Dai, Z. Ou, and Q. Tang. Calibration of a multiple axes 3-D laser scanning system consisting of robot, portable laser scanner and turntable. *Optik - International Journal for Light and Electron Optics*, **122**(4):324 – 329, 2011.

[Li13] Y. Li, X. Fan, N. Mitra, D. Chamovitz, D. Cohen-Or, and B. Chen. Analyzing growing plants from 4D point cloud data. *ACM Trans. on Graphics*, **32**(6), Nov. 2013.

[Park05] S. Park and M. Subbarao. A multiview 3D modeling system based on stereo vision techniques. *Machine Vision and Applications*, **16**(3):148–156, 2005.

[Rusi01] S. Rusinkiewicz and M. Levoy. Efficient variants of the ICP algorithm. *Proc. Int'l Conf. on 3D Digital Imaging and Modeling*, pp. 145–152, 2001.

[Sadl05] F. Sadlo, T. Weyrich, R. Peikert, and M. Gross. A practical structured light acquisition system for point-based geometry and texture. *Proc. EG/IEEE VGTC Symp. on Point-Based Graphics*, pp. 89–145, June 2005.

[Sain04] M. Sainz, R. Pajarola, A. Mercade, and A. Susin. A simple approach for point-based object capturing and rendering. *IEEE Computer Graphics and Applications*, **24**(4):24–33, July 2004.

[Xian04] T. Xian, S. Park, and M. Subbarao. New dynamic zoom calibration technique for a stereo-vision based multi-view 3D modeling system. *Proc. SPIE*, Vol. **5606**, 2004.

Xufang Pang received her B.Sc. degree from Jiamusi University and her M.Sc. degree from Nanjing Normal University, in 2007 and 2010, respectively. She is now a Research Assistant in the Department of Computer Science of City University of Hong Kong. Her research interests include digital geometry processing, computer graphics and machine learning.

Rynson Lau received his B.Sc. honors degree from University of Kent and his Ph.D. degree from University of Cambridge. He has been on the faculty of Durham University, City University of Hong Kong, and The Hong Kong Polytechnic University. He is currently with the City University of Hong Kong. Rynson serves on the Editorial Board of Computer Animation and Virtual Worlds, and IEEE Trans. on Learning Technologies. He has served as the Guest Editor of a number of journal special issues, including IEEE Internet Computing, ACM Trans. on Internet Technology, IEEE Trans. on Multimedia, IEEE Trans. on Visualization and Computer Graphics, and IEEE Computer Graphics & Applications. In addition, he has also served in the committee of a number of conferences, including Program Co-chair of ACM VRST 2004, ICWL 2005, ICEC 2007, ACM MTDL 2009, IEEE U-Media 2010, and Conference Co-chair of CASA 2005, ACM VRST 2005, ICWL 2007, IDET 2008, ACM MDI 2009, ACM MTDL 2010, ACM VRST 2010. His research interests include computer graphics and distributed virtual environments.

Zhan SONG received Ph.D. in Mechanical and Automation Engineering from the Chinese University of Hong Kong, Hong Kong, in 2008. He is currently with the Shenzhen Institutes of Advanced Technology (SIAT), Chinese Academy of Sciences (CAS), as a professor. His current research interests include structured-light based sensing, image processing, 3-D face recognition, and human-computer interaction.

Yangyan Li is a Post-Doc in the Geometric Computing group of Stanford University. He received his Ph.D. degree from Shenzhen Institutes of Advanced Technology, Chinese Academy of Sciences in 2013. His major research interest lies in point cloud based reconstruction.

Shengfeng He received the B.Sc. and the M.Sc. degree in the Faculty of Information Technology from Macau University of Science and Technology in 2009 and 2011, respectively. He is now a Ph.D. student in the Department of Computer Science of City University of Hong Kong. His research interests include image processing, computer vision, computer graphics, physically-based animation and machine learning.

Contact Information

Xufang Pang

Address: Department of Computer Science, City University of Hong Kong, Tat Chee Avenue, Kowloon, Hong Kong.

Phone: (852) 6850-3542, (852) 3442-2029

Email: pangxufang@gmail.com

Rynson W.H. Lau

Address: Department of Computer Science, City University of Hong Kong, Tat Chee Avenue, Kowloon, Hong Kong

Phone: (852) 3442-7525

Email: rynson.lau@cityu.edu.hk

Zhan Song

Address: Rm B301, Shenzhen Institutes of Advanced Technology, No. 1068, Xueyuan Avenue, University Town, Xili, Nanshan District, Shenzhen, China, 518055

Phone: (86) 755-86392100

Fax: (86) 755-86392194

Email: zhan.song@siat.ac.cn

Yangyan Li

Address: 4321 Collins Ct, Apt 8, Mountain View, CA 94040, United States

Phone: (1) (650)-422-8090

Email: yangyan.lee@gmail.com

Shengfeng He

Address: Department of Computer Science, City University of Hong Kong, Tat Chee Avenue, Kowloon, Hong Kong.

Phone: (852) 5305-5189

Email: shengfeng_he@yahoo.com